Continuous PWM Techniques for Sinusoidal Voltage Generation with Seven-Phase Voltage Source Inverters

D.Dujic, E.Levi, M.Jones
Liverpool John Moores University
School of Engineering
Liverpool L3 3AF, UK
d.dujic@2006.ljmu.ac.uk

G.Grandi, G.Serra, A.Tani
University of Bologna
Department of Electrical Engineering
40136 - Bologna, Italy
gabriele.grandi@mail.ing.unibo.it

***Abstract* – Multi-phase motor drives are typically supplied from two-level voltage source inverters (VSIs). It is thus necessary to develop pulse width modulation (PWM) schemes for inverter control in order to utilise the benefits offered by multi-phase motor drives. This paper deals with seven-phase VSI and develops continuous PWM schemes that enable generation of sinusoidal voltages at the output. Carrier-based sinusoidal PWM, sinusoidal PWM with the 7th harmonic injection, and sinusoidal PWM with the triangular zero-sequence injection, as well as the space vector PWM are elaborated. Presented PWM schemes are analysed in terms of DC bus utilisation and direct correlation between carrier-based and space vector approach is established. All schemes are implemented in a digital signal processor and are compared through experimentation on a seven-phase custom-designed VSI supplying a seven-phase star-connected static load.**

I. Introduction

Multi-phase drives have certain advantages that make them attractive for electric ship propulsion, locomotive traction, EVs, HEVs, etc. Regardless of the AC machine type and regardless of the number of phases, the power supply of a multiphase drive is typically a two-level VSI, which requires a method of PWM for its operation. If a multi-phase machine is with sinusoidal field distribution, PWM scheme must generate sinusoidal harmonic-free output voltages in order to avoid appearance of low-order stator current harmonics [1]. However, if a multi-phase machine is with concentrated windings, it is advantageous to supply the machine with a voltage that contains, in addition to the fundamental, a certain amount of harmonic(s) of a specified order, so that stator current harmonic injection enhances torque production [2-3].

Numerous PWM schemes for multi-phase VSIs have already been reported [1-14]. Most of the work has been related to space vector PWM. Carrier-based PWM methods have been analysed to a lesser extent [10-12,14]. From the point of view of the VSI phase number, [3-6] deal with space vector PWM of the five-phase VSI, [1,2,13,14] with asymmetrical six-phase VSI, and [7] with symmetrical six-phase VSI. PWM strategies for a seven-phase and a nine-phase VSI, respectively, are discussed in [8] and [9].

An extension of symmetrical component transformation on multi-phase systems leads to definition of multiple voltage space vectors positioned in different mutually orthogonal *d-q* planes of an *n*-dimensional space. This is a generalisation of the approach of [1] and it enables decoupling of fundamental and harmonic components into different planes, which simplifies further control implementation. Sinusoidal output voltage generation in the case of an *n*-phase system requires application of *n*-1 active space vectors in a switching period [9]. If sinusoidal voltage output is required, only the first d_1-q_1 plane (sub-space) has to be considered.

As noted, PWM for a seven-phase VSI has been considered only in [8], where space vector PWM was developed. Although carrier-based PWM methods are in general easier to implement when compared to the space vector approach, there is no evidence that such an approach has been followed in conjunction with the seven-phase VSI. However, as shown in [10], injection of the n^{th}-harmonic (zero-sequence) into reference signals in case of an *n*-phase system effectively increases linear modulation region without affecting output voltage waveforms and enables the same DC voltage utilisation as the space vector PWM [10]. The aim of this paper is therefore to investigate a set of continuous PWM methods for sinusoidal output voltage generation using seven-phase VSI. Three sinusoidal carrier-based methods (sinusoidal PWM, sinusoidal PWM with the 7th harmonic injection, and sinusoidal PWM with the triangular zero-sequence injection) are compared with space vector PWM that produces sinusoidal voltages in order to determine direct link between these approaches. All the methods are implemented in a DSP and tested on a seven-phase VSI supplying a seven-phase load. Experimental results are presented, thus enabling a comparison of carrier-based and space-vector PWM methods.

II. Seven-Phase Voltage Source Inverter

Topology of a seven-phase voltage source inverter supplying seven-phase star-connected load is given in Fig. 1. By defining switching functions m_i $(i = a,b,c,d,e,f,g)$ for inverter legs with $m_i = 1$ and $m_i = 0$ when upper switch is 'on' and 'off', respectively, instantaneous values of phase-to-neutral voltages of a seven-phase load can be calculated using the following expressions

$$v_i = V_{dc}\left[m_i - \frac{1}{7}(m_a + m_b + m_c + m_d + m_e + m_f + m_g) \right] \quad (1)$$

There are 2^7 = 128 switching configurations during operation of a seven-phase VSI. Since only linear modulation region is under scope of interest here, modulation index is defined as the ratio of the fundamental component amplitude of the line-to-neutral inverter output voltage to one half of the DC bus voltage,

$$M_i = V_1 / 0.5V_{dc} \quad (2)$$

III. Continuous Carrier-Based PWM for Seven-Phase VSI

Carrier-based PWM techniques include modulation signals and carrier signals. Generalised structure of the modulator, including zero-sequence signal calculator, is shown in Fig. 2. Modulation signals are compared with high frequency carrier signal and, as a result, switching signals are generated for each phase. A universal representation of modulation signals for seven-phase carrier-based modulator can be written as

$$v_i(t) = v_i^*(t) + v_{no}(t) \quad (3)$$

where $v_{no}(t)$ represents zero-sequence signal and $v_i^*(t)$ are fundamental signals (seven sinusoidal signals displaced in time by $\alpha = 2\pi/7$). Since zero-sequence signal does not appear in either line-to-line or phase voltages, selection of this signal can be used to modify modulation signal waveforms. This is a degree of freedom that can be utilised to design various modulation schemes. Analysis is here restricted to continuous PWM schemes with switching activity in each of the inverter legs over the carrier signal period, as long as peak value of the modulation signal does not exceed carrier magnitude. For the sake of simplicity in the analysis, amplitude of carrier signal is scaled to fit into range $(-V_{dc}/2 \div V_{dc}/2)$ and its frequency is assumed to be much higher than the frequency of fundamental signals. While operating in linear regime modulator gain has the unity value and peak value of inverter output fundamental voltage is equal to the peak value of the fundamental sinusoidal signal.

Sinusoidal Pulse Width Modulation – SPWM: Selection of zero-sequence signal as $v_{no}(t) = 0$ leads to SPWM. Modulation signals for all seven phases are equal to sinusoidal fundamental signals. In the linear region, the maximum modulation index is equal to unity, $M_{SPWM} = 1$.

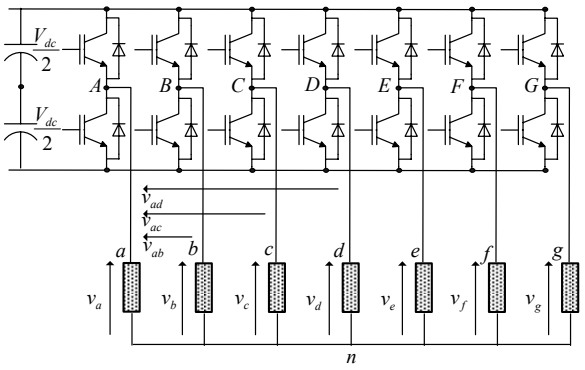

Fig. 1. Topology of a seven-phase voltage source inverter.

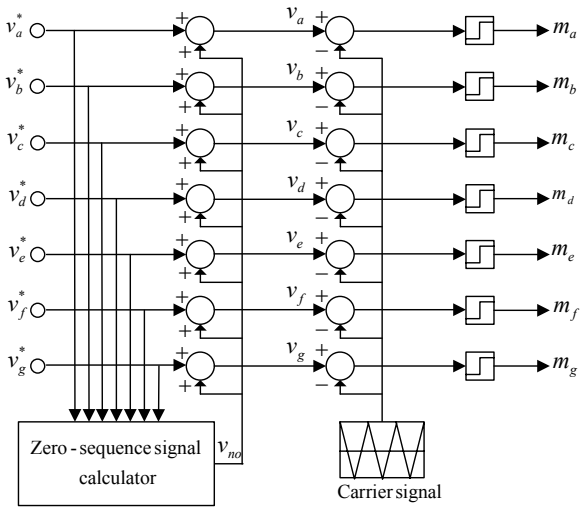

Fig. 2. Principle of carrier-based PWM for a seven-phase VSI.

SPWM with Seventh Harmonic Injection – SHIPWM: Third-harmonic injection for a three-phase VSI leads to an increase in the DC bus utilisation in the linear region. A generalised concept of n^{th} harmonic injection for *n*-phase inverters [10] is applied here to the seven-phase VSI. Optimal level of the n^{th} harmonic component is found from:

$$V_n = \pm V_1 \sin(\pi/2n)/n \quad (4)$$

where (4) takes the positive sign for *n* = (3, 7, 11, 15…) and negative sign for *n* = (5, 9, 13, 17…). Thus, for a seven-phase system, the seventh harmonic is in phase with the fundamental and has the amplitude:

$$V_7 = V_1 \sin(\pi/14)/7 \approx 0.0318 * V_1 \quad (5)$$

With zero-sequence signal defined by $v_{no}(t) = V_7 \sin(7\omega t)$, the resulting modulating signal has the form (phase *a*)

$$v_a(t) = M_i * 0.5V_{dc} \sin(\omega t) + 0.0318 M_i * 0.5V_{dc} \sin(7\omega t) \quad (6)$$

In the linear region, for maximum value of the modulation index, one has $|v_a(t)| = 0.5V_{dc}$. General expression for maximum possible modulation index in the linear region in case of the n^{th} harmonic injection has the form [10]

$$M_i = 1/\cos(\pi/2n) \quad (7)$$

from where it can be found that maximum value of the modulation index is $M_{SHIPWM} = 1.0257$. This is an increase of 2.57% in the DC bus utilisation when compared to SPWM.

SPWM with Triangular Zero-Sequence Injection – TIPWM: If the zero-sequence is selected according to

$$v_{no}(t) = -\frac{1}{2}[\max(v_a^*, v_b^*, \ldots v_g^*) + \min(v_a^*, v_b^*, \ldots v_g^*)] \quad (8)$$

not just the seventh harmonic, but additional 7*k* (*k* = 1,3,5...) harmonics are included into the modulation signal as well. Maximum modulation index has the value equal to the one in the previous case, $M_{TIPWM} = 1.0257$. Characteristic waveforms of SHIPWM and TIPWM schemes are shown in Fig. 3. Similarity in waveforms is obvious. Additional 7*k* harmonics are naturally included, thus leading to triangular

shape of the zero-sequence signal in TIPWM. Plots show situation for maximum value of the modulation index, thus fundamental signal exceeds unity value, while resulting modulation signal stays inside the linear region.

IV. Space Vector PWM for Seven-Phase VSI (SVPWM)

By using transformation in real matrix form as

$$C=\frac{2}{7}\begin{bmatrix} 1 & \cos(\alpha) & \cos(2\alpha) & \cos(3\alpha) & \cos(4\alpha) & \cos(5\alpha) & \cos(6\alpha) \\ 0 & \sin(\alpha) & \sin(2\alpha) & \sin(3\alpha) & \sin(4\alpha) & \sin(5\alpha) & \sin(6\alpha) \\ 1 & \cos(2\alpha) & \cos(4\alpha) & \cos(6\alpha) & \cos(\alpha) & \cos(3\alpha) & \cos(5\alpha) \\ 0 & \sin(2\alpha) & \sin(4\alpha) & \sin(6\alpha) & \sin(\alpha) & \sin(3\alpha) & \sin(5\alpha) \\ 1 & \cos(3\alpha) & \cos(6\alpha) & \cos(2\alpha) & \cos(5\alpha) & \cos(\alpha) & \cos(4\alpha) \\ 0 & \sin(3\alpha) & \sin(6\alpha) & \sin(2\alpha) & \sin(5\alpha) & \sin(\alpha) & \sin(4\alpha) \\ 1/2 & 1/2 & 1/2 & 1/2 & 1/2 & 1/2 & 1/2 \end{bmatrix} \quad (9)$$

decomposition of a seven-phase system into components in three two-dimensional and mutually orthogonal planes (single dimensional zero-sequence sub-space can not be excited due to the isolated neutral of the star-connected load) can be realised. Applying (9) to phase-to-neutral voltages of a seven-phase load determined with (1), all 128 space vectors (two zero and 126 active space vectors) of a seven-phase system are determined. In general, space vectors occupy the same positions in all three planes, that are labelled here d_1-q_1, d_2-q_2 and d_3-q_3, although one switching combination of the inverter leads to a different space vector in each plane with regard to the magnitude and phase. Considering the magnitudes, active space vectors can be classified into eight groups [8], while each plane can be divided into 14 sectors (each spanning π/7), as shown in Fig. 4. Transforming voltages of a seven-phase VSI into three two-dimensional planes effectively separates families of odd harmonics according to the rule:

- $7k \pm 1$ harmonics, k = even → d_1–q_1 plane, (**1**, 13, 15,...).
- $7k \pm 2$ harmonics, k = odd → d_2–q_2 plane, (**5**, 9, 19,…).
- $7k \pm 3$ harmonics, k = even → d_3–q_3 plane, (**3**, 11, 17,…).
- $7k$ harmonics, k = odd → zero-sequence (**7**, 21, 35,…).

Therefore, as long as pure sinusoidal output voltages are required, space vector modulator must eliminate all harmonic components in the d_2-q_2 and d_3-q_3 planes, while realising fundamental component synthesis in d_1-q_1 plane.

Neighbouring n–1 active space vectors are selected in each sector [8,9], thus providing symmetrical PWM pattern with single commutation in each inverter leg over the switching

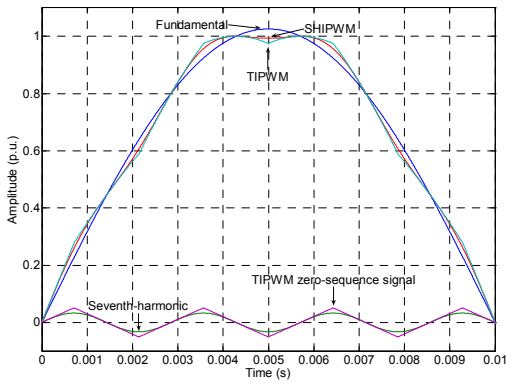

Fig. 3. Characteristic signals of carrier-based PWM methods.

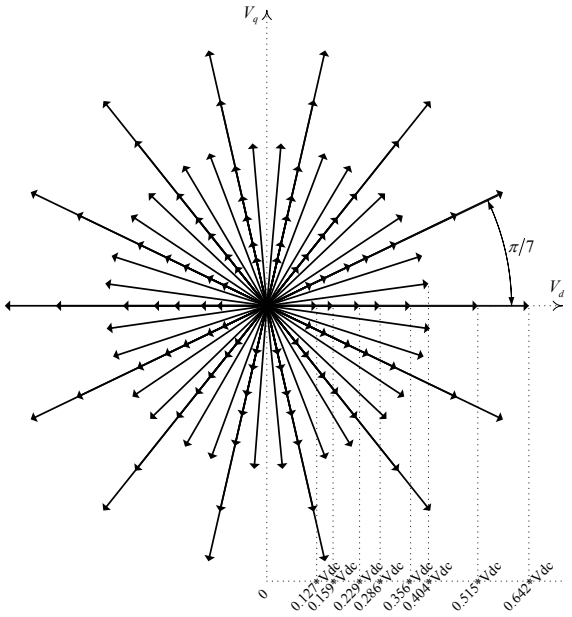

Fig. 4. Space vectors of seven-phase VSI.

period, starting from (0000000) up to (1111111) and vice versa. Since selected active space vectors are along same two lines that separate the sectors, fictional space vectors $\bar{v}_a$ and $\bar{v}_b$ can be used at first to simplify calculation (Fig. 5a). This is the same as assuming that only space vectors with the largest magnitude are involved in the PWM pattern. Such an approach, based on [5] for a five-phase VSI, is followed here and it is different from the previously proposed methodology for the seven-phase VSI in [8]. Ultimately, however, both methods lead to the same output voltages. Application times of vectors $\bar{v}_a$ and $\bar{v}_b$ can be found for any sector j from

$$t_a=\frac{|\bar{v}^*|\sin(j\pi/7-\vartheta)}{|\bar{v}_L|\sin(\pi/7)}t_s, \quad t_b=\frac{|\bar{v}^*|\sin(\vartheta-(j-1)\pi/7)}{|\bar{v}_L|\sin(\pi/7)}t_s \quad (10)$$

where $|\bar{v}_L|=0.642V_{dc}$ represents magnitude of the largest space vector group from Fig. 4 while t_s is the switching period. Time of application of zero space vectors is

$$t_o=t_s-t_a-t_b \quad (11)$$

Calculated times of application of fictional space vectors $\bar{v}_a$ and $\bar{v}_b$ must be properly distributed among active space vectors, satisfying constraints given with

$$t_a=t_{a1}+t_{a2}+t_{a3} \qquad t_b=t_{b1}+t_{b2}+t_{b3} \quad (12)$$

In sector 1 active space vectors that are used are $\bar{v}_{64},\bar{v}_{115},\bar{v}_{97},\bar{v}_{123},\bar{v}_{96},\bar{v}_{113}$ (Fig. 5b), where number in subscript represents decimal value of binary coded inverter switching state (e.g. 64 = 1000000). Positions and amplitudes of these vectors in other two planes are shown in Figs. 5c and 5d. In order to eliminate low-order harmonic components in inverter output voltages, average values in planes d_2-q_2 and d_3-q_3 must be kept at zero. Thus, from Fig. 5c, for d_2-q_2 plane the following constraints apply

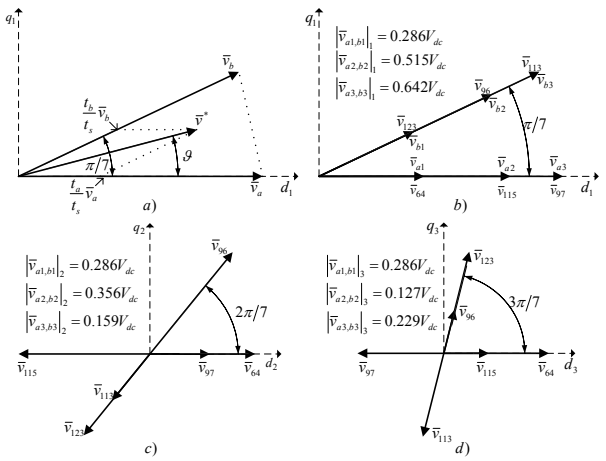

Fig. 5. Principle of calculation of times of application of active space vectors (parts a,b,c,d defined in text).

$$t_{a1}\left|\overline{v}_{a1}\right|_2 + t_{a3}\left|\overline{v}_{a3}\right|_2 = t_{a2}\left|\overline{v}_{a2}\right|_2$$
$$t_{b1}\left|\overline{v}_{b1}\right|_2 + t_{b3}\left|\overline{v}_{b3}\right|_2 = t_{b2}\left|\overline{v}_{b2}\right|_2 \qquad (13)$$

Similarly, for d_3-q_3 plane, from Fig. 5d one finds

$$t_{a1}\left|\overline{v}_{a1}\right|_3 + t_{a2}\left|\overline{v}_{a2}\right|_3 = t_{a3}\left|\overline{v}_{a3}\right|_3$$
$$t_{b1}\left|\overline{v}_{b1}\right|_3 + t_{b2}\left|\overline{v}_{b2}\right|_3 = t_{b3}\left|\overline{v}_{b3}\right|_3 \qquad (14)$$

After solving system (12)-(14) dwell factors for active space vectors are obtained as:

$$t_{a1} = 0.198 * t_a \qquad t_{b1} = 0.198 * t_b$$
$$t_{a2} = 0.357 * t_a \qquad t_{b2} = 0.357 * t_b \qquad (15)$$
$$t_{a3} = 0.445 * t_a \qquad t_{b3} = 0.445 * t_b$$

By using the volt-second principle [5] it can be shown that for any given reference magnitude the corresponding fundamental at the output is only 82%. This is so since the calculation of times in (10) corresponds to the maximum fundamental achievable with large vectors only ($0.6259V_{dc}$), while application of six active vectors according to (15) restricts the maximum achievable fundamental to $0.513V_{dc}$. The ratio of the two maximum fundamentals is 1.22. Thus the reference voltage magnitude has to be scaled with the factor 1/0.82 = 1.22 in order to get the desired fundamental at the output.

Obtained switching pattern for sector 1 is shown in Fig. 6. Time of application of zero space vectors is equally shared between $\overline{v}_0$ and $\overline{v}_{127}$.

V. Experimental Results

All four PWM schemes are implemented in the TMS320F2812 DSP that is used to control seven-phase VSI (Fig. 7) supplying a seven-phase star-connected R-L load. DC link voltage is obtained using single-phase diode rectifier and is 345 V. Measurements are done for the fundamental output frequency of 50 Hz and the inverter switching frequency is 10 kHz. Load current and its spectrum were measured using Tektronix current probe and HP35665A dynamic signal analyser, DSP outputs with Tektronix TDS 2014 digital scope and inverter output voltages with FLUKE 43B power harmonic analyser in oscilloscope mode.

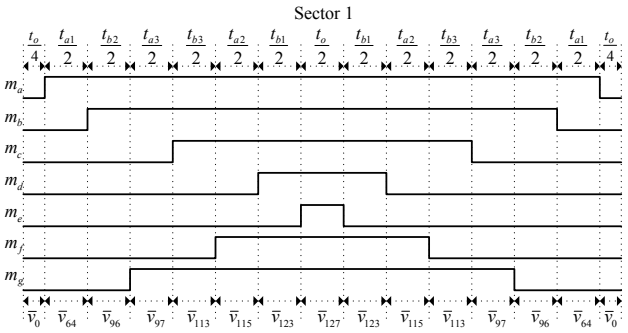

Fig. 6. Switching pattern for sector 1.

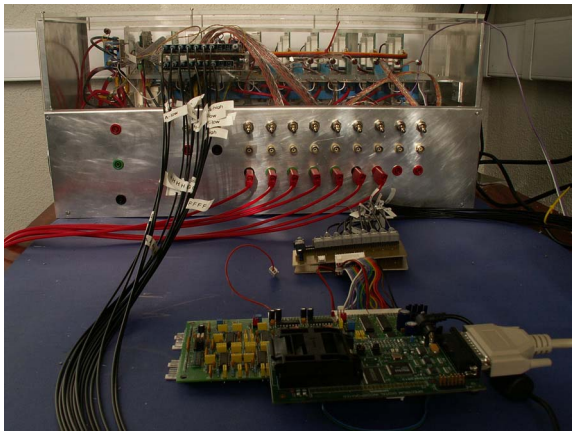

Fig. 7. Experimental set-up.

On the basis of the theoretical considerations it is expected that, during operation with the maximum modulation index value in the linear region, three of the considered four PWM methods will provide the same fundamental at the output (SHIPWM, TIPWM and SVPWM), while the output of the SPWM will be slightly lower. This is confirmed in Fig. 8, where one period of the load current is shown for all four PWM methods. Further evidence is provided by harmonic analysis (Fig. 9), where current spectrum is illustrated for sinusoidal PWM (SPWM) and the SPWM with triangular zero-sequence injection (TIPWM) (current spectrum for SHIPWM and SVPWM is identical to the one shown for

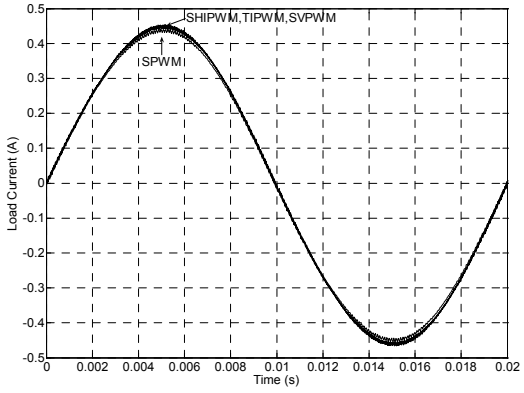

Fig. 8. Measured load current for all four PWM methods for operation with the maximum fundamental in the linear modulation region (50 Hz reference frequency).

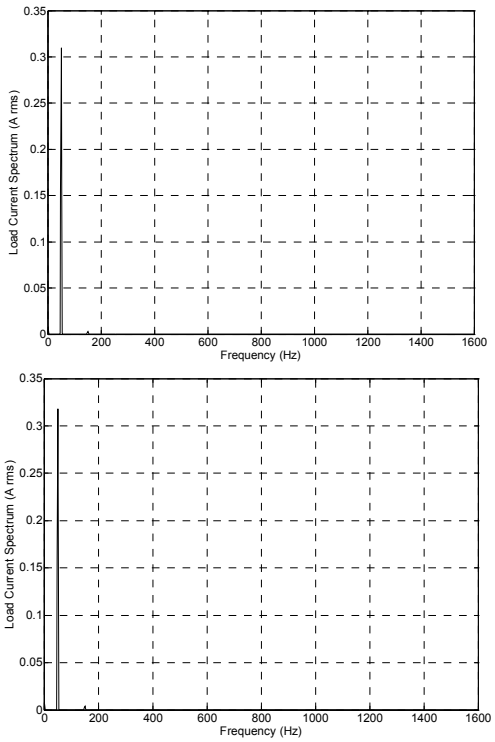

Fig. 9. Spectrum of load current of Fig. 8 for SPWM (top) and carrier-based space vector PWM (TIPWM, bottom).

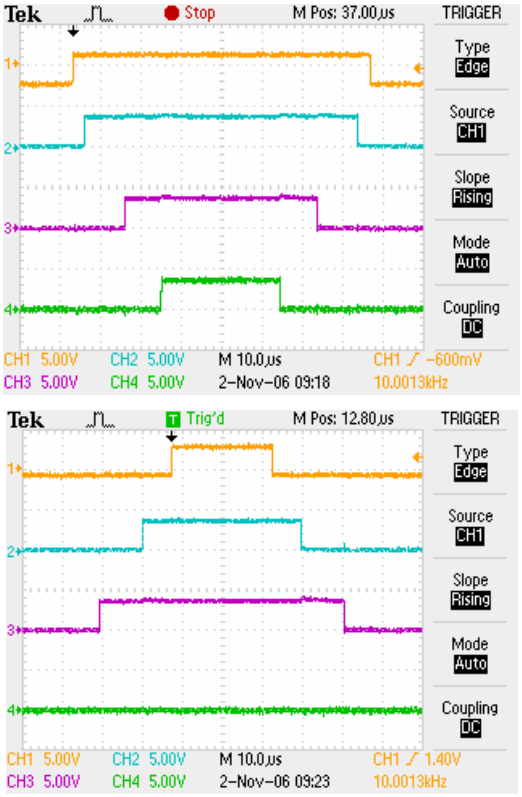

Fig. 10. Switching pattern for space vector PWM (SVPWM) using six active vectors, during one switching period in sector 1. Inverter legs *A*, *B*, *C* and D in upper part and inverter legs *E*, *F* and *G* in lower part.

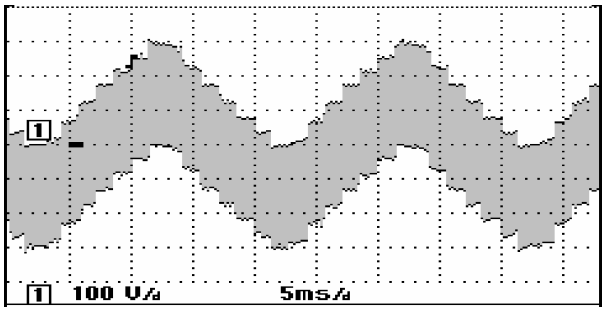

Fig. 11. Measured inverter output phase voltage, generated using SVPWM in the limit of the linear modulation region.

TIPWM). It can be seen from the spectra that an increase in the fundamental current harmonic, commensurate with the increase in the fundamental output voltage harmonic in the linear modulation region of 2.57%, has been obtained with TIPWM (the same applies to SHIPWM and SVPWM), when compared to the fundamental for sinusoidal PWM.

Considering that SHIPWM, TIPWM and SVPWM all lead to in essence the same output voltage/current, voltage is further illustrated for SVPWM only, for operation in the limit of the linear modulation region. Switching pattern, generated by the SVPWM during one switching period and measured at the DSP outputs, is illustrated for all seven inverter legs during operation in sector 1 in Fig. 10. As can be seen, PWM pattern is symmetrical and six active vectors are applied, in agreement with theoretical considerations. Inverter output phase voltage is shown in Fig. 11. It attains six different non-zero voltage levels, in accordance with (1).

Maximum fundamental output phase voltage in the linear modulation region for SHIPWM, TIPWM and SVPWM equals $0.513V_{dc}$ for sinusoidal output voltages. This is well below the maximum fundamental that can be obtained in the limit of the linear modulation if only the largest vectors of Fig. 4 are utilised, which is then $0.6259V_{dc}$. Such operation of the seven-phase VSI corresponds to the injection of not only zero-sequence harmonics but also harmonics in the d_2-q_2 and d_3-q_3 planes (the 3rd and the 5th harmonic). Inverter output current when only the largest space vectors are used in the SVPWM, for operation in the limit of the linear modulation region, is illustrated in Fig. 12, together with the spectrum. As can be seen, the current contains around 25% and 10% of the 3rd and the 5th harmonic, respectively. This is undesirable if a machine with sinusoidal winding distribution is supplied. Direct comparison of the load current waveforms, obtained using only two largest active vectors (Fig. 12) and six active vectors (Fig. 8), is provided in Fig. 13, from which the difference in both harmonic content and the magnitude is evident.

The final set of experimental results, shown in Fig. 14, illustrates common mode voltage (CMV). Waveform is shown for operation with the maximum fundamental output in the linear modulation region for SVPWM. The same result was obtained for SPWM. The CMV fluctuates between $\pm V_{dc}/2$ and it contains all voltage levels.

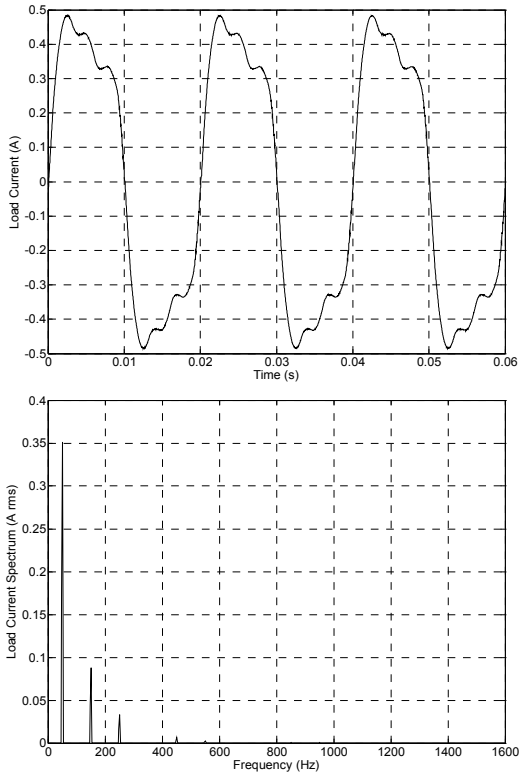

Fig. 12. Experimentally recorded current and its spectrum when only the largest vectors are used in SVPWM (limit of the linear modulation region, voltage fundamental of $0.6259V_{dc}$).

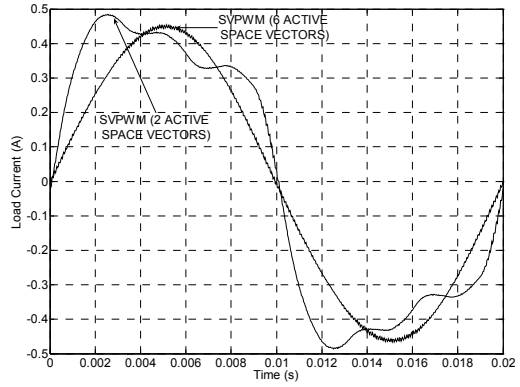

Fig. 13. Comparison of the load current for SVPWM using six active vectors and SVPWM using only two active vectors.

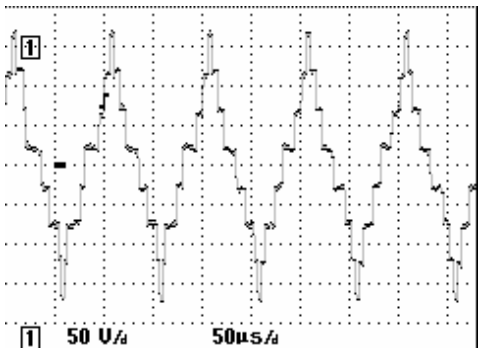

Fig. 14. CMV recorded for operation with the maximum sinusoidal output in the linear modulation region using SVPWM.

VI. Conclusion

The paper analyses continuous PWM schemes for seven-phase voltage source inverters, which enable operation with purely sinusoidal output voltages. Carrier-based schemes (sinusoidal, sinusoidal with the 7th harmonic injection and sinusoidal with triangular zero-sequence injection), as well as the space vector PWM are elaborated. It is shown that SHIPWM, TIPWM and SVPWM all enable an increase in the maximum obtainable fundamental output in the linear modulation region, of 2.57%, compared to the simplest carrier-based sinusoidal PWM. Theoretical considerations are confirmed by experimentation on the seven-phase VSI.

Acknowledgment

The authors acknowledge support provided by the EPSRC (grant no. EP/C007395), Semikron, MOOG and Verteco.

References

[1] Y.Zhao, T.A.Lipo, "Space vector PWM control of dual three-phase induction machine using vector space decomposition," *IEEE Trans. on Industry Applications,* vol. 31, no. 5, 1995, pp. 1100-1109.

[2] R.O.C.Lyra, T.A.Lipo, " Torque density improvement in a six-phase induction motor with third harmonic current injection," *IEEE Trans. on Industry Applications,* vol. 38, no. 5, 2002, pp. 1351-1360.

[3] H.M.Ryu, J.H.Kim, S.K.Sul, "Analysis of multi-phase space vector pulse width modulation based on multiple d-q spaces concept," *IEEE Trans. on Power Electronics,* vol. 20, no. 6, 2005, 1364-1371.

[4] P.S.N.deSilva, J.E.Fletcher, B.W.Williams, "Development of space vector modulation strategies for five-phase voltage source inverters," *Proc. IEE Power Electronics, Machines and Drives Conf. PEMD,* Edinburgh, UK, 2004, pp. 650-655.

[5] A.Iqbal, E.Levi, "Space vector PWM techniques for sinusoidal output voltage generation with a five-phase voltage source inverter," *Electric Power Components and Systems,* vol. 34, no. 2, 2006, pp. 119-140.

[6] D.Casadei. G.Serra, A.Tani, L.Zarri, "Multi-phase inverter modulation strategies based on duty-cycle space vector approach," *Proc. of Ship Propulsion and Railway Systems Conf. SPRTS*, Bologna, Italy, 2005, pp. 222-229.

[7] M.B.R.Correa, C.B.Jacobina, C.R.daSilva, A.M.N.Lima, E.R.C.da Silva, "Vector and scalar modulation for six-phase voltage source inverters," *Proc. IEEE Power Elec. Spec. Conf. PESC*, Acapulco, Mexico, 2003, pp. 562–567.

[8] G.Grandi, G.Serra, A.Tani, "Space vector modulation of a seven-phase voltage source inverter," *Proc. Int. Symp. Power Electronics, Elec. Drives, Automation and Motion SPEEDAM,* Taormina, Italy, 2006, CD-ROM paper S8-6.

[9] J.W.Kelly, E.G.Strangas, J.M.Miller, "Multi-phase space vector pulse width modulation," *IEEE Trans. on Energy Conversion,* vol. 18, no. 2, 2003, pp. 259-264.

[10] A.Iqbal, E.Levi, M.Jones, S.N.Vukosavic, "Generalised sinusoidal PWM with harmonic injection for multi-phase VSIs," *Proc. IEEE Power Elec. Spec. Conf. PESC,* Jeju, Korea, 2006, pp. 2871-2877.

[11] O.Ojo, G.Dong, "Generalized discontinuous carrier-based PWM modulation scheme for multi-phase converter-machine systems," *Proc. IEEE Ind. Appl. Soc. Annual Meeting IAS,* Hong Kong, 2005, CD-ROM paper IAS38p3.

[12] O.Ojo, G.Dong, Z.Wu, "Pulse-width modulation for five-phase converters based on device turn-on times," *Proc. IEEE Ind. Appl. Soc. Annual Meeting IAS*, Tampa, FL, 2006, CD-ROM paper IAS15p7.

[13] D.Hadiouche, L.Baghli, A.Rezzoug, "Space vector PWM techniques for dual three-phase AC machine: Analysis, performance evaluation and DSP implementation," *IEEE Trans. on Industry Applications*, vol. 42, no. 4, 2006, pp. 1112-1122.

[14] R.Bojoi, A.Tenconi, F.Profumo, G.Griva, D.Martinello, "Complete analysis and comparative study of digital modulation techniques for dual three-phase AC motor drives," *Proc. IEEE Power Elec. Spec. Conf. PESC*, Cairns, Australia, 2002, CD-ROM paper 10159.